6. Trunk, G., Heerten, A., Poul, A. and Reuter, E., Geogrid wrapped vibro, stone columns. In EuroGeo3: Geotech. Eng. with Geosynthetics, Munich, Germany, 2004, pp. 289–294.
7. Ayadat, T. and Hanna, A. M., Encapsulated stone columns as a soil improvement technique for collapsible soil. *Ground Improvement*, 2005, **4**(9), 137–147.
8. Di Prisco, C., Galli, A., Cantarelli, E. and Bongiorno, D., Georeinforced sand columns: small scale experimental tests and theoretical modeling. In Proceedings of the 8th International Conference on Geosynthetics, Yokohama, Japan, 2006, pp. 1685–1688.
9. Lee, D., Yoo, C. and Park, S., Model tests for analysis of load carrying capacity of geogrid encased stone column. In the Proceedings of the 17th International Offshore and Polar Engineering Conference, Lisbon, Portugal, 2007, pp. 1631–1635.
10. Murugesan, S. and Rajagopal, K., Model tests on geosynthetic encased stone columns, *Geosynth. Int*, 2007, **14**(6), 346–354.
11. Murugesan, S. and Rajagopal, K., Studies on the behavior of single and group of geosynthetic encased stone columns. *J. Geotech. Geoenviron. Eng.*, 2010, **136**(1), 129–139.
12. Murugesan, S. and Rajagopal, K., Shear load tests on stone columns with and without geosynthetic encasement. *J. Geotech. Testing*, 2008, **32**(1), 1–10.
13. Gniel, J. and Bouazza, A., Improvement of soft soils using geogrid encased stone columns. *Geotext. Geomembr.*, 2009, **27**(3), 167–175.
14. Wu, C. S. and Hong, Y. S., Laboratory tests on geosynthetic encapsulated sand columns. *Geotext. Geomembr.*, 2009, **27**(2), 107–120.
15. Gniel, J. and Bouazza, A., Construction of geogrid encased stone columns: a new proposal based on laboratory testing. *Geotext. Geomembr.*, 2010, **28**, 108–118.
16. Murugesan, S. and Rajagopal, K., Geosynthetic-encased stone columns: numerical evaluation. *Geotext. Geomembr.*, 2006, **24**(6), 349–358.
17. Malarvizhi, S. N. and Ilamparuthi, K., Comparative study on the performance of encased stone column and conventional stone column. *Soils Found.*, 2007, **47**(5), 873–885.
18. Khabbazian, M., Kaliakin, V. N. and Meehan, C. L., Numerical study of the effect of geosynthetic encasement on the behaviour of granular columns. *Geosynth. Int.*, 2010, **17**(3), 132–143.
19. Yoo, C. and Kim, S. B., Numerical modeling of geosynthetic encased stone column-reinforced ground. *Geosynth. Int.*, 2009, **16**(3), 116–126.
20. Yoo, C., Performance of geosynthetic-encased stone columns in embankment construction: numerical investigation. *J. Geotech. Geoenviron. Eng.*, 2010, **136**(8), 1148–1160.
21. Brinkgreve, R. B. and Vermeer, P. A., *PLAXIS 3D-Finite Element Code for Soil and Rocks Analysis*, A.A. Balkema, Rotterdam Brookfield, 2010.
22. Ambily, A. P. and Gandhi, S. R., Behavior of stone columns based on experimental and FEM analysis. *J. Geotech. Geoenviron. Eng.*, 2007, **133**(4), 405–415.
23. Mustafa, V., Mustafa, A., Banu, S., Ikizler, C. and Umit, C., Experimental and numerical investigation of slope stabilization by stone columns. *Nat. Hazards*, 2012, **64**, 797–820.

ACKNOWLEDGEMENT. We thank Mr Paresh Patel (Unique Construction, Surat) for providing financial support for the laboratory work.

Received 14 October 2014; revised accepted 15 December 2014

On the vertical wavelength estimates using the Krassovsky parameters of OH airglow monitoring

R. N. Ghodpage[1,*], A. Taori[2], P. T. Patil[1], Devendraa Siingh[3], S. Gurubaran[4] and A. K. Sharma[5]

[1]Medium Frequency Radar, Indian Institute of Geomagnetism, Shivaji University Campus, Kolhapur 416 004, India
[2]National Atmospheric Research Laboratory, Gadanki 517 112, India
[3]Indian Institute of Tropical Meteorology, Pune 411 008, India
[4]Indian Institute of Geomagnetism, Navi Mumbai 410 218, India
[5]Department of Physics, Shivaji University, Kolhapur 416 004, India

The photometric measurements of mesospheric OH and O(^{1}S) emission, carried out from Kolhapur (16.8°N, 74.2°E), Maharashtra during January–April 2005 are used to study the wave characteristics. The nocturnal variability reveals the dominant long-period wave signatures with significant amplitudes of embedded short-period waves. We carry out a sensitivity study on the vertical wavelength (VW) derived with the help of Krassovsky parameters ($\eta = |\eta|e^{i\Phi}$) of the OH data, which reveals VW to vary from 38.9 to 110.2 km. This was compared with the VW estimates using the phase difference of the simultaneously observed waves in both OH and O(^{1}S) emission intensities. Results reveal that in the absence of attitudinally resolved measurements, the VW estimated using Krassovsky method can be used.

Keywords: Airglow, atmospheric gravity waves, lower thermosphere, mesosphere, vertical wavelength.

ATMOSPHERIC gravity waves (AGWs) play a significant role in the dynamics features of the mesosphere and lower thermosphere (MLT) region by transporting energy and momentum horizontally and vertically upward and also providing dynamical linkage between the lower atmosphere and the MLT region. Multispectral nightglow emissions recorded at low-latitude stations showed the presence of gravity waves with periods ranging from a few minutes to a few hours[1,2]. Ground-based airglow emissions are widely used to study the short-period (tens of minutes) waves with short horizontal wavelength (tens of kilometres)[3–7]. Hecht *et al.*[8] showed the presence of long-period (~2 h) and large horizontal wavelength (~300–400 km) gravity waves as well as short-period (15–25 min) and small horizontal wavelength (~30–45 km) gravity waves in the airglow data over Alice Spring, Australia. The short-period waves might have been trapped/ducted by thermal ducts and took several hours to reach the mesopause region. Snively *et al.*[7] reported that airglow perturbations of small-scale ducted gravity waves near the Brunt–Vaisala period are primarily

*For correspondence. (e-mail: rupeshghodpage@gmail.com)

determined by density perturbations of minor species (O_3 and H) by short wave period. Also, they found that for ducted wave the phase of Krassovsky ratio was a function of both the phase of the wave dynamics perturbations and the position of the packet relative to the gradients of minor species participating in the photochemistry.

Based on numerical simulation results, Snively and Pasko[9] showed that upward propagating gravity waves generated by tropospheric convection broke near the mesopause altitude, excited short-period secondary waves, which were trapped in the upper mesosphere and lower thermosphere due to local maximum of Brunt–Vaisala frequency. The primary waves with period near 10 min, excited by a tropospheric oscillator broke and excited new secondary gravity waves with period near 5 min, which became trapped in the thermospheric duct. These wave structures clearly resemble quasi-monochromatic structures commonly observed in airglow measurements[3,10–17].

The propagation of the gravity waves also influences the photochemistry by affecting the concentration of the chemically active constituents and the local temperatures. Evidence of temporal and spatial structures has been observed in the mesospheric OH, O(^{1}S) and O_2 airglow and such structures have been related to the passage of atmospheric internal gravity waves[18]. Studies concerning gravity wave propagation in the middle and upper atmosphere reveal that it plays an important role in energy and momentum transport and further global energy balance in the upper atmosphere[19–21].

Interaction of upward propagating waves and the ambient imprints of these process in the dynamical variability, which is noted in the observed airglow intensity and temperature perturbations[18]. Assuming the wave perturbations to be adiabatic, the dynamical effects can be quantified by the Krassovsky ratio[11] denoted as η; this is quantified as the ratio of normalized intensity perturbations to the associated normalized temperature perturbations of a particular wave. Later modelling studies[12,13,18] have defined this parameter as $\eta = |\eta| e^{i\Phi}$, where $|\eta|$ is the ratio between the emission intensity and temperature perturbation amplitudes of the wave normalized to their time averages, and Φ is the phase difference between the intensity wave and its temperature counterpart. We can also estimate the VW (λz) with the help of Krassovsky parameters[13]

$$\lambda z = \frac{2\pi\gamma H}{(\gamma - 1)|\eta| \sin\phi}, \tag{1}$$

where $\gamma = C_p/C_v = 1.4$ is the ratio of specific heats, and $H = 6$ km is the scale height. Equation (1) is valid for the zenith observation of the plane waves but it is not valid for the evanescent waves.

Many observational as well as theoretical studies have wave characterization using the Krassovsky method[12,22–36]. One of the advantages of Krassovsky analysis is that we can infer VW of an upward propagating wave with single-altitude OH airglow measurements. However, there have been no efforts so far validating these estimates. The present communication compares the direct VW estimate using the simultaneous OH and O(^{1}S) emission monitoring with the one calculated using the Krassovsky parameters.

The multispectral photometer monitors airglow emissions at 840 and 846 nm rotational lines of OH (6, 2), O(^{1}S) 557.7 nm and O(^{1}D) 630 nm emissions near simultaneously. The low temperature coefficient interference filters (10 cm aperture) used in the photometer have ~1 nm full width at half maximum with transmission efficiency ~30–65% at 24°C. The photometer has F/2 optics with a full field of view ~10°. As the stepper motor rotates, a filter wheel keeps each filter in the field-of-view one by one. The stepper motor rotation and home position sensing are controlled by the computer. The photomultiplier tube, EMI9658B is used as a detector. A high-gain trans-impedance amplifier is used in the signal amplification in order to convert the weak (nA) output current of the photomultiplier into corresponding voltage form. Output is further recorded in the computer in analogue format in terms of arbitrary units along with time. The aim of the present study is to compare the mesospheric wave characteristics; hence only OH measurements are taken. More details of the multispectral photometer are presented elsewhere[36].

In the present study we have used only those nights which have more than 6 h of good observations during January–April 2005.

To understand the wave structures, we analyse the mesospheric OH emission data obtained over Kolhapur (16.8°N, 74.2°E), Maharashtra during January–April 2005. We use the perturbation amplitudes normalized to their time-averaged values in the intensity and temperature data to calculate the Krassovsky parameters. A typical example of nocturnal variability in the mesospheric OH emissions on 8 and 9 January 2005 is shown in Figure 1. The mean deviations of intensity and temperature data are shown in Figure 1 *a* and *b* respectively, while the intensity and temperature residuals are shown in Figure 1 *c* and *d* respectively. We note that night airglow intensity variations show a long-period wave with superposed large amplitude short-period oscillatory features. On this night, the average of OH band airglow intensity is found to be ~7.58 arbitrary units and average of the temperature data ~201.3 K. In particular, temperature data on this night exhibit large peak-to-peak variations of about 40 K. To characterize the nocturnal variability, together with data we plot the results (shown as red solid lines) of best-fit cosine model[31,37] as follows

$$Y = A\cos\left[\pi\frac{(X - Xc)}{T}\right], \tag{2}$$

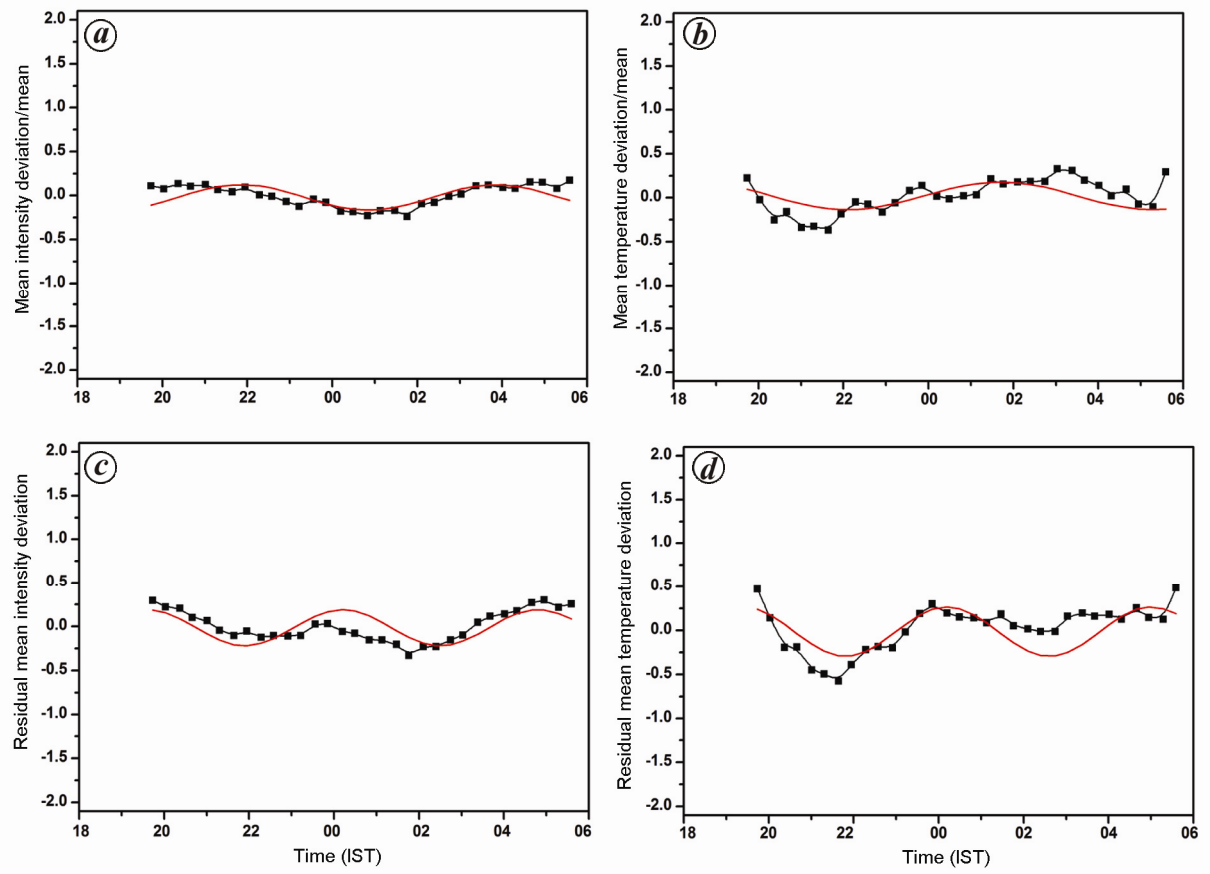

Figure 1. Nocturnal variability in the mesospheric OH emissions on 8 and 9 January 2005 at Kolhapur. ***a***, ***b***, Mean deviations in intensity and temperature. ***c***, ***d***, Intensity and temperature residuals. Solid red line in each plot show the result of simple best-fit cosine model which estimates the dominant wave periodicity, amplitude and phase of waves obtained over Kolhapur.

where A is the amplitude of the fitted wave of half period T with phase Xc at time X. Solid line curves in each plot show the result of this model. We can see that best-fitted ~6.9 ± 1.5 h wave represents long-period nocturnal variability in the intensity data and 7.4 ± 1 h in temperature data. Looking at the uncertainties in the estimate of wave periods, we treat this to be a signature of a same wave with period (average) ~7.1 ± 1.8 h with relative amplitudes ~6.0% and 0.9% respectively, in intensity and temperature data. This results in the $|\eta|$ value of 6.7 ± 0.18 for the observed 7.1 h principal wave. Further, to find the second dominant wave, we subtract the best-fit model data from the normalized mean deviation data and obtain the residuals (Figure 1 *c* and *d*). The solid red lines show the results of the best-fit analysis carried out on the residual data. It is clear that dominant residual waves in the intensity and temperature data have ~4.6 and 4.8 h periods respectively (i.e. 4.7 h wave periods). The best-fit analysis also shows the relative percentage amplitudes of this wave to be ~0.70% and 1.33% in the temperature and intensity data respectively. Thus, the $|\eta|$ value for residual waves is estimated to be 1.9 ± 0.94.

The phase difference between the intensity and temperature waves is obtained by cross-correlation analysis between intensity and temperature wave (fitted) data. We note that the phase of the principal waves (maxima; period ~7.1 h) is 25.3 h (i.e. ~1.3 h) in the temperature-fitted data and 21.95 h in the intensity-fitted data, which results in the phase difference of ~–3.32 h, i.e. the Φ value is −167.5° ± 3°. Similarly, for the residual/shorter period (periodicity ~4.8 h) the Φ value is estimated to be –53.5° ± 31°. Using these values and eq. (1), we find the VWs to be –110.2 ± 14 km and –94.5 ± 40 km for the principal and residual waves respectively (negative sign represents upward propagation of VWs).

Figure 2 depicts the O(^{1}S) emission variability noted on 8 and 9 January 2005. Figure 2 *a* plots the mean intensity deviations of O(^{1}S) emission (normalized to their mean intensity values). The period noted in the O(^{1}S) emission is 7.6 ± 1.2 h, which is in reasonable agreement with the wave period noted in the OH emission (7.1 h). The residual intensity variations in O(^{1}S) emission are plotted in Figure 2 *b*. The wave period is found to be 4.8 ± 0.9 h, which is similar to the observed residual wave period in the OH data. Assuming the peak emission altitudes of OH and O(^{1}S) layer to be ~87 and 97 km respectively, using the observed phase of the waves in OH and O(^{1}S) emissions, we can calculate the VWs of the

Table 1. Estimated values of the wave parameters from OH emission and O(^{1}S) data during January to April 2005

Date	Wave period OH (h)	Wave period O (^{1}S) (h)	$\|\eta\|$ – OH	Phase difference OH (intensity – temperature) (degrees)	Vertical wavelength (km)	
					Using Krassovsky parameter	Using O(^{1}S) and OH phase difference
6 January	7.6 ± 1.6	8.0 ± 1.7	4.46 ± 0.20	–160 ± 10	86.4 ± 5	37.8
	3.8 ± 1.1	4.2 ± 0.9	1.45 ± 0.25	–91.7 ± 10	90.4 ± 8	50.4
7 January	8.0 ± 1.5	7.2 ± 1.2	3.47 ± 0.10	–157 ± 12	96.0 ± 35	127.5
	3.6 ± 0.4	3.6 ± 0.3	1.88 ± 0.15	–97 ± 5	76.2 ± 2	24.6
8 January	7.1 ± 1.8	7.6 ± 1.2	5.50 ± 0.18	–167.5 ± 3	110.2 ± 4	123.8
	4.8 ± 0.6	4.8 ± 0.4	1.73 ± 0.94	–53.5 ± 31	94.5 ± 40	94.3
10 January	5.2 ± 1.3	6.6 ± 1.7	4.50 ± 0.30	–23 ± 05	75 ± 20	85.4
	3.6 ± 0.3	3.6 ± 0.4	2.40 ± 0.98	–213 ± 10	101 ± 50	99.0
11 January	6.4 ± 1.6	7.1 ± 0.9	2.80 ± 0.69	–151.8 ± 35	99.3 ± 38	41.4
	4.0 ± 1.0	3.6 ± 0.8	2.10 ± 1.1	–101.3 ± 20	64.0 ± 42	27.8
14 January	6.0 ± 1.4	6.6 ± 1.1	5.60 ± 0.51	–162 ± 40	75.8 ± 40	51.2
	3.6 ± 0.4	3.7 ± 0.3	2.30 ± 1.05	–99 ± 33	58.1 ± 45	40.8
5 February	7.2 ± 0.9	7.6 ± 0.8	5.50 ± 1.20	–153 ± 5	62.3 ± 7	52.1
	2.6 ± 0.5	2.8 ± 0.7	2.41 ± 1.42	–83.7 ± 20	55.5 ± 10	39.2
8 February	5.2 ± 0.8	5.8 ± 1.1	5.72 ± 0.91	–162.4 ± 40	75.9 ± 48	25.1
	2.6 ± 0.2	2.9 ± 0.3	2.60 ± 1.14	–101.8 ± 5	51 ± 36	28.9
9 February	7.8 ± 1.1	7.1 ± 1.2	6.10 ± 1.15	–152.6 ± 48	46.8 ± 32	85.8
	3.9 ± 0.7	3.4 ± 0.4	3.87 ± 1.28	–60.2 ± 20	38.9 ± 8	30.3
10 February	8.0 ± 0.9	8.0 ± 0.7	4.10 ± 2.50	–49.4 ± 10	42.3 ± 15	55.7
	4.0 ± 0.3	4.0 ± 1.1	1.80 ± 1.0	–92.8 ± 10	73.3 ± 48	34.9
7 March	7.0 ± 0.4	7.0 ± 0.8	2.51 ± 1.08	–149.4 ± 12	103.3 ± 45	76.2
	4.2 ± 0.9	3.6 ± 1.3	1.61 ± 0.50	–85.4 ± 22	82.7 ± 12	53.2
8 March	7.2 ± 1.1	6.8 ± 1.4	4.01 ± 0.9	–23.2 ± 8	83.4 ± 10	69.4
	2.8 ± 1.2	3.6 ± 0.8	1.90 ± 0.70	–79.5 ± 32	70.6 ± 20	58.4
9 March	6.4 ± 1.8	7.2 ± 1.5	5.50 ± 0.50	–156.4 ± 40	59.7 ± 25	88.0
	2.4 ± 0.8	3.2 ± 1.2	2.20 ± 0.75	–87 ± 30	64.7 ± 21	39.4
10 April	7.1 ± 1.1	7.9 ± 1.8	3.10 ± 1.80	–34.5 ± 20	75.2 ± 12	84.0
	3.7 ± 0.6	3.1 ± 0.8	2.40 ± 1.2	–86.4 ± 18	55.1 ± 14	40.7

waves[15]. We obtain the phase difference between the OH and O(^{1}S) emission intensity with the cross-correlation analysis on the fitted waves. The phase of the principal waves (minima; period ~7.2 h) is 25.3 h (i.e. 1.6 h) in the OH data and 24.6 h in the O(^{1}S) emission data, which results in the phase difference of ~0.6 h and hence the corresponding phase delay value is ~32°. Similarly, for the shorter period (periodicity ~4.8 h), the phase delay value is estimated to be ~42°. Thus, computed vertical wavelengths for the principal and residual waves are 123.7 ± 15 and 94.2 ± 5 km respectively. Note that these values are close to those estimated using eq. (1).

We carried out a similar analysis on all 14 nights when conspicuous wave signatures were noted both in intensity and temperature data; the results are shown in Table 1. We note that principal nocturnal waves in the data show wave periods to vary from 5 to 8.2 h with corresponding temperature amplitudes ranging from 0.7% to 11.8%. However, the intensity amplitudes of the principal waves vary from 2.3% to 65.2%. Thus calculated $|\eta|$ values are found to range from 2.2 to 6.1 for the principal wave. In case of residual waves, periodicity varies from 2.2 to 4.8 h, with corresponding temperature amplitude ranging from 0.5% to 6.0%; while the intensity amplitudes varied from ~1.1% to 10%. Hence, the calculated $|\eta|$ values for short-period waves are found to range from 1.5 to 3.8. The phase Φ values also exhibit large variability for long-period (and short-period) waves, which vary from –23° to –167.5° (and –53° to –213.5°). The deduced vertical wavelengths are found to vary from 40 to 124 km and 28 to 100 km for the principal and residual waves respectively.

The calculated η and Φ values are plotted in Figure 3, which shows a large spread in the distribution. A similar spread in the distribution of observed values of η has also been observed[26,29–30,38–43]. Our values agree well with the reported measurements of Hecht and Walterscheid[26]. It is noteworthy that Reisin and Scheer[30] found mean (arithmetic) values of η to be 5.5 ± 0.6 and Φ values to be –66° for OH emissions. Our observed values of η (arithmetic mean, 5.01 ± 1.09) match well with these values. In a further report, based on 5-year observations, Reisin and Scheer[41] found the mean η of ~5.6 for the nightly long-period waves and ~3.4 for the waves having 1000 s periods; which is also in agreement with our values. Further, based on long-term observations with a spectral airglow temperature imager (SATI) from a mid-latitude station, Lopez-Gonzalez *et al.*[43] reported a mean η of approximately ~8.6 for the OH data. Guharay *et al.*[33] found that for wave periods ranging from 6 to 13 h, η varies from

1.7 to 5.4, while Φ varies from –13° to –90°. Guharay *et al.*[32] noted that the periodicity of ~8–10 h of Krassovsky parameters for the principal wave (~10 h periodicity) was found to be 15.5 ± 4.4 on 15 January and 4.6 ± 1.0 on 16 January for OH. Similarly, Aushev *et al.*[44] showed the amplitude of Krassovsky parameters (for wave periods 2.2 to 4.7 h) to vary from 2.4 to 3.6 and Φ to vary from –63° to –121°. A large spread in the η and Φ values may be due to (a) the oxygen profile variability[45] from one place to other, (b) the dependency of η on the [O] distribution, (c) complex OH chemistry[46] and (d) sensitivity arising because of the peak emission altitude variation[36].

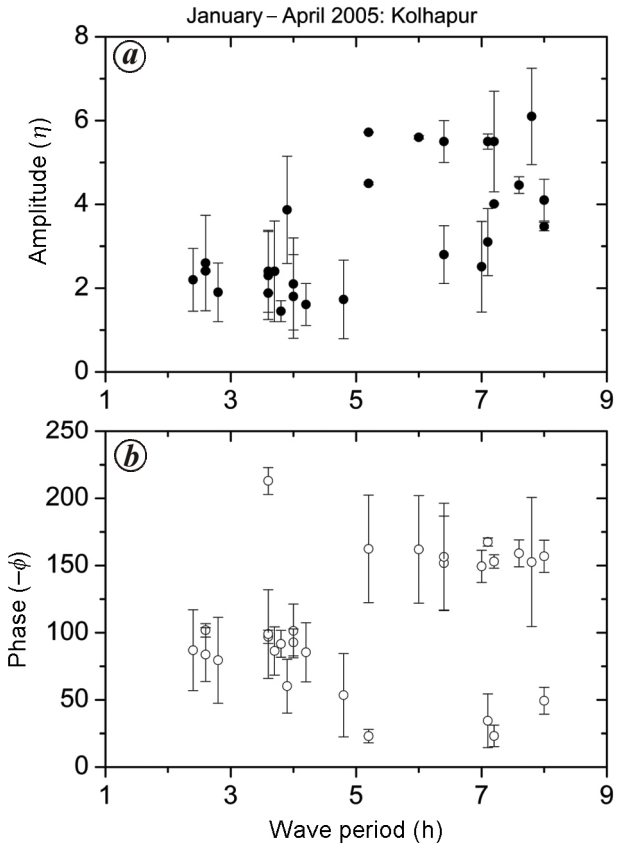

Figure 2. ***a***, Distribution of amplitude η variation of Krassovsky parameters with respect to the observed wave periods. ***b***, Distribution of phase Φ of Krassovsky parameters with respect to the observed wave periods.

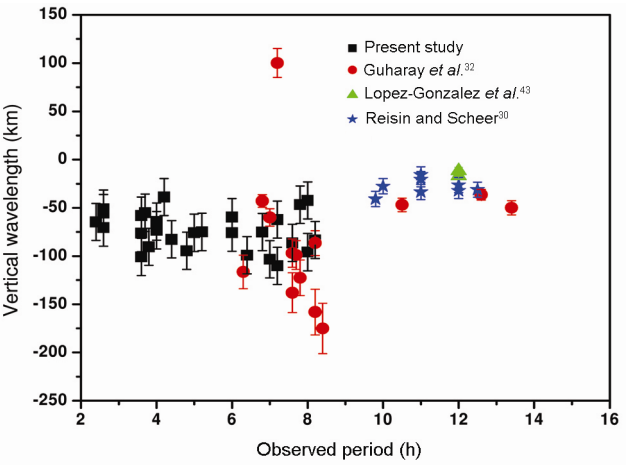

Figure 3. Deduced vertical wavelength for the observed waves as a function of their periods with a comparison with values obtained by other researchers.

Figure 4 shows the derived VW for all the observations explained above using eq. (1). It can be seen from the figure that there exist large variations from one night to another. The plot depicts a large range of VWs from 40 to 124 km in case of the principal waves, and 28 to 100 km for the residual waves. The mean VW values for long- and short-period waves are calculated to be –72.3 ± 41 and –59.5 ± 35 km respectively. All the observations show negative values of λ_z, indicating an upward propagation. Further, unlike the clear dependency on the wave period noted in the Krassovsky parameters (η and Φ), no clear trend is noted in the calculated VW. It is noteworthy that for all the nights VW for the principal wave is higher than that of residual waves. For a comparison, we also

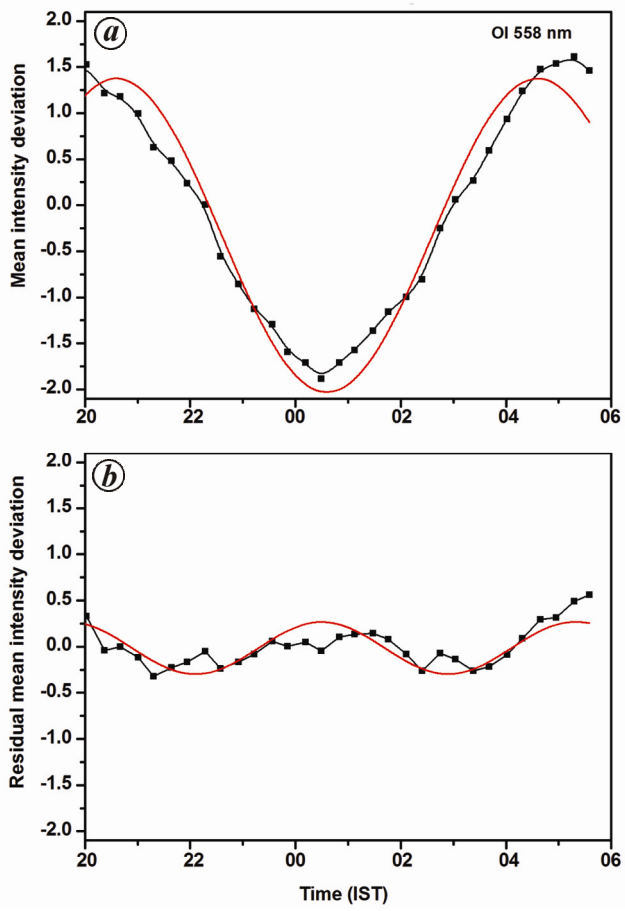

Figure 4. Nocturnal variability in O(^{1}S) 557.7 nm emissions on 8 and 9 January 2005. ***a***, ***b***, Mean deviations in intensity and intensity residuals. Solid red lines in each plot show the result of simple best-fit cosine model.

show the values reported by Reisin and Scheer[30], Lopez-Gonzalez *et al.*[43], and Guharay *et al.*[32]. Our values lie well within the ranges reported by other investigators. Reisin and Scheer[30] found a mean VW for OH of approximately –30 km with about 2.8 km variability, which is in agreement with our values. The observed VW values of Guharay *et al.*[32] lie within the range of our observed values. However, Lopez-Gonzalez *et al.*[43] observed VW values to be approximately –10 km for OH, which does not agree with our values. Recently, from a similar location, Ghodpage *et al.*[36] reported the observed vertical wavelengths to vary from 28.6 to 163 km, which is in agreement with the present values. Further, Takahashi *et al.*[34] reported the VWs to vary from 20 to 80 km, which is also in agreement with our results. Unique to the present study is the estimation of VWs of waves having short periods compared to the previous studies which have reported VWs of waves which had periods more than 6 h.

Table 1 compares the VW values obtained by eq. (1) with those calculated by the waves noted in OH and O(^{1}S) emissions. Here we consider the VW values derived using OH and O(^{1}S) representing direct estimates as we use the phase difference of waves noted in two different airglow emissions. The assumption here is that altitude variation on a given night is not large enough to affect the separation between the OH and O(^{1}S) emission layers. The values obtained from eq. (1) are derived based on the Krassovsky parameters at single airglow emission altitude. We note that there are some differences in these two estimates. To quantify the validity of VWs obtained by Krassovsky parameters, Figure 5 plots these two estimates and also calculates the correlation coefficients between them. The solid red line shows the result

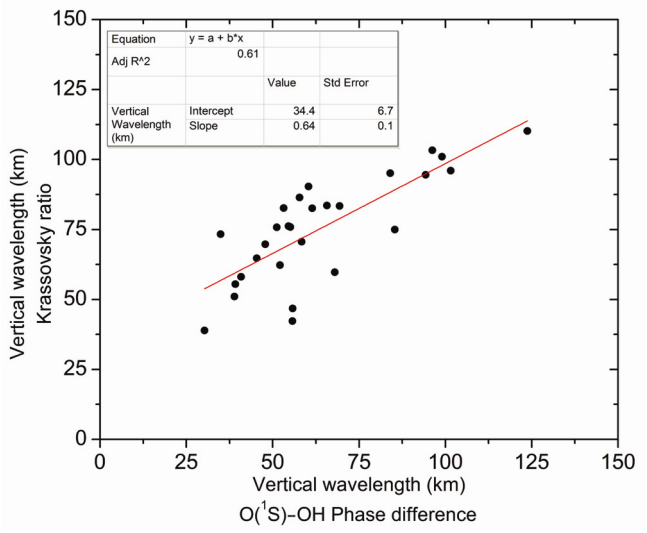

Figure 5. Comparison of the deduced vertical wavelength values of the observed waves obtained with the help of Krassovsky parameters for OH emissions and phase difference of waves noted in OH and O(^{1}S) emissions.

of the least squares linear-fitting. The R^2 value is estimated to be 0.61, which suggests that there exist a correlation between them. It suggests that the method of VW calculation using the Krassovsky parameters provides a reasonable values. The absence of a strong correlation is partially because in the calculations we have assumed: (a) propagation of gravity wave from OH layer to the O(^{1}S) layer without any nonlinear interaction, (b) the altitudes of these layers do not vary and (c) effects of photochemical processes do not vary. Therefore, the assumptions need not be real. The fact that an earlier study[47] has shown that peak emission altitudes of OH and O(^{1}S) emissions may change by ±2 km, can bring as large as 20% difference in the estimated VWs by the direct method. The variability brought in by the photochemistry can influence the Krassovsky ratio which may also provide significant differences[14,45,48]. However, in spite of these limitations, our results suggest that in the case when multiple airglow emission monitoring is not available, VWs estimated by Krassovsky parameters can provide reasonable estimates.

Our results are summarized as follows:

(i) The data show the dominance of upward propagating wave with periods ranging from 2.2 to 8.2 h in the mesospheric OH temperature as well as intensity and that there are exists a large spread in the estimated values of Krassovsky parameters.

(ii) The $|\eta|$ values are found to be large for the long-period waves and comparatively small for the short-period waves and vary from 1.5 to 6.1. The Φ values also show a similar trend and vary from –23° to –167.5°.

(iii) Observed VW values for all the nights of the observation show large variations from one night to another and vary from –38.5 to –110 km using Krassovsky parameters.

(iv) A good agreement between the VWs estimated using multiple emission airglow monitoring and Krassovsky parameters shows the usefulness of the latter.

In conclusion, Krassovsky parameters provide a useful tool to study the long VW waves. The present study validates this with two simultaneous airglow emissions occurring at upper mesospheric altitudes.

1. Molina, A., Lopez-Puestas, Lopez-Moreno, J. J. and Rodrigo, R., Gravity waves from five simultaneous emissions: OH (6–2), NaD, $O_2(^1\Sigma)$, OI–557.7 nm, and the visible continuum. *Can. J. Phys.*, 1985, **63**, 592–596.
2. Takahashi, H., Batista, P. P., Sahai, Y. and Clemesha, B. R., Atmospheric wave propagations in the mesopause region observed by the OH (8,3) band, NaD, O_2A (8645 A) band and OI 5577 A emissions. *Planet. Space Sci.*, 1985, **33**, 381.
3. Nakamura, T., Higashikawa, A., Tsuda, T. and Matsushita, Y., Seasonal variations of gravity wave structures in OH airglow with

a CCD imager at Shigaraki. *Earth Planets Space*, 1999, **51**, 897–906.
4. Hecht, J. H., Walterscheid, R. L., Hickey, M. and Franke, S., Climatology and modeling of quasi-monochromatic atmospheric gravity waves observed over Urbana Illinois. *J. Geophys. Res.*, 2001, **106**(D6), 5181–5195.
5. Hecht, J. H., Kovalam, S., May, P. T., Mills, G., Vincent, R. A., Walterscheid, R. L. and Woithe, J., Airglow imager observations of atmospheric gravity waves at Alice Springs and Adelaide, Australia during the Darwin Area Wave Experiment (DAWEX). *J. Geophys. Res.*, 2004, **109**, D20S05; doi:10.1029/2004JD004697.
6. Pautet, P.-D., Taylor, M. J., Liu, A. Z. and Swenson, G. R., Climatology of short-period gravity waves observed over northern Australia during the Darwin Area Wave Experiment (DAWEX) and their dominant source regions. *J. Geophys. Res.*, 2005, **110**, D03S90; doi:10.1029/2004JD004954.
7. Snively, J., Pasko, V. and Taylor, M., OH and OI airglow layer modulation by ducted short period gravity waves: Effects of trapping altitude. *J. Geophys. Res.*, 2010, **115**, A11311; doi: 10.1029/2009JA015236.
8. Hecht, J. H. *et al.*, Imaging of atmospheric gravity waves in the stratosphere and upper mesosphere using satellite and ground-based observations over Australia during the TWPICE campaign. *J. Geophys. Res.*, 2009, **114**, D18123; doi:10.1029/2008JD011259.
9. Snively, J. B. and Pasko, V. P., Breaking of thunderstorm-generated gravity waves as a source of short-period ducted waves at mesopause altitudes. *Geophys. Res. Lett.*, 2003, **30**, 2254; doi: 10.1029/2003GL018436.
10. Taylor, M. J., Hapgood, M. A. and Rothwell, P., Observations of gravity wave propagation in the OI (557.7 nm), Na (589.2 nm) and the near infrared OH emissions. *Planet. Space Sci.*, 1987, **35**, 413.
11. Krassovsky, V. I., Infrasonic variation of OH emission in the upper atmosphere. *Ann. Geophys.*, 1972, **28**, 739–746.
12. Hines, C. O. and Tarasick, D. W., On the detection and utilization of gravity waves in airglow studies. *Planet. Space Sci.*, 1987, **35**, 851–866.
13. Tarasick, D. W. and Hines, C. O., The observable effects of gravity waves in airglow emission. *Planet. Space Sci.*, 1990, **8**, 1105–1119.
14. Tarasick, D. W. and Shepherd, G. G., Effects of gravity waves on complex airglow chemistries: 2. OH emission. *J. Geophys. Res.*, 1992, **97**, 3195–3208.
15. Fagundes, P. R., Takahashi, H., Sahai, Y. and Gobbi, D., Observations of gravity waves from multi-spectral mesospheric nightglow emissions observed at 23°S. *J. Atmos. Terr. Phys.*, 1995, **57**, 395–405.
16. Ghodpage, R. N., Siingh, D., Singh, R. P., Mukherjee, G. K., Vohat, P. and Singh, A. K., Tidal and gravity waves study from the airglow measurements at Kolhapur (India). *J. Earth Syst. Sci.*, 2012, **121**, 1511–1525.
17. Siingh, D., Singh, R. P., Singh, A. K., Kumar, S., Kulkarni, M. N. and Singh, A. K., Discharge in stratosphere and mesosphere. *Space Sci. Rev.*, 2012, **169**, 73–121; DOI:10.1007/s11214-012-9906-0.
18. Hines, C. O., A fundamental theorem of airglow fluctuations induced by gravity waves. *J. Atmos. Sol.–Terr. Phys.*, 1997, **59**, 319–326.
19. Manson, A. H. and Meek, C. E., Gravity wave propagation characteristics (60–120 km) as determined by the Saskatoon MF radar (Gravnet) system 1983–1985 at 52°N. *J. Atmos. Sci.*, 1988, **45**, 932–946.
20. Kato, S., Earth's atmosphere in dynamic coupling envisaged through atmospheric tides and atmospheric gravity waves: a view on the past–present–future research. *J. Geophys. Res. A*, 1996, **101**, 10577–10585.
21. Taori, A. and Taylor, M., Dominant winter-time mesospheric wave signatures over a low latitude station, Hawaii (20.8°N): an investigation. *J. Earth Syst. Sci.*, 2010, **119**(3), 259–264.
22. Hecht, J. H., Walterscheid, R. L., Sivjee, G. G., Christensen, A. B. and Pranke, J. B., Observations of wave-driven fluctuations of OH nightglow emission from Sondre Stromfjord, Greenland. *J. Geophys. Res. A*, 1987, **92**(6), 6091–6099.
23. Walterscheid, R. L., Schubert, G. and Straus, J. M., A dynamical chemical model of wave driven fluctuations in the OH nightglow. *J. Geophys. Res.*, 1987, **92**, 1241–1254.
24. Hickey, M. P., Effects of eddy viscosity and thermal conduction and Coriolis force in the dynamics of gravity wave driven fluctuations in the OH nightglow. *J. Geophys. Res.*, 1988, **93**, 4077–4088.
25. Hickey, M. P., Wavelength dependence of eddy dissipation and coriolis force in the dynamics of gravity wave driven fluctuations in the OH nightglow. *J. Geophys. Res.*, 1988, **93**, 4089–4101.
26. Hecht, J. H. and Walterscheid, R. L., Observations of the OH meinel (6, 2) and O_2 atmospheric (0, 1) night glow emissions from Maui during the ALOHA-90 campaign. *Geophys. Res. Lett.*, 1991, **18**(7), 1341–1344.
27. Lowe, R. P., Gilbert, K. L. and Turnbull, D. N., High latitude summer observations of the hydroxyl air glow. *Planet. Space Sci.*, 1991, **39**, 1263–1270.
28. Taylor, M. J., Espy, P. J., Baker, D. J., Sica, R. J., Nea, P. C. and Pendleton Jr, W. R., Simultaneous intensity, temperature and imaging measurements of short period wave structure in the OH nightglow emission. *Planet. Space Sci.*, 1991, **39**, 1171–1188.
29. Takahashi, H., Sahai, Y., Batista, P. P. and Clemesha, B. R., Atmospheric gravity wave effect on the airglow O_2 (0-1) and OH (9-4) band intensity and temperature variations observed from a low latitude station. *Adv. Space Res.*, 1992, **12**(10), 131–134.
30. Reisin, E. R. and Scheer, J., Characteristics of atmospheric waves in the tidal period range derived from zenith observations of O_2 (0-1) Atmospheric and OH (6-2) airglow at lower mid-latitudes. *J. Geophys. Res.*, 1996, **101**, 21223–21232.
31. Taori, A. and Taylor, M., Characteristics of wave induced oscillations in mesospheric O_2 emission intensity and temperatures. *Geophys. Res. Lett.*, 2006, **33**, L01813; doi:10.1029/2005GL024442.
32. Guharay, A., Taori, A. and Taylor, M., Summer-time nocturnal wave characteristics in mesospheric OH and O_2 airglow emissions. *Earth Planet Space*, 2008, **60**, 973–979.
33. Guharay, A., Taori, A., Bhattacharjee, B., Pant, P., Pande, P. and Pandey, K., First ground-based mesospheric measurements from central Himalayas. *Curr. Sci.*, 2009, **97**(5), 664–669.
34. Takahashi, H., Onohara, A., Shiokawa, K., Vargas, F. and Gobbi, D., Atmospheric wave induced O_2 and OH airglow intensity variations: effect of vertical wavelength and damping. *Ann. Geophys.*, 2011, **29**, 631–637.
35. Taori, A., Kamalakar, V., Raghunath, K., Rao, S. V. B. and Russell III, J. M., Simultaneous Rayleigh lidar and airglow measurements of middle atmospheric waves over low latitudes in India. *J. Atmos. Sol.–Terr. Phys.*, 2012, **78**, 62–69; doi:10.1016/j.jastp.2011.06.012.
36. Ghodpage, R. N., Taori, A., Patil, P. T. and Gurubaran, S., Simultaneous mesospheric gravity wave measurements in OH night airglow emission from Gadanki and Kolhapur – Indian low latitudes. *Curr. Sci.*, 2013, **104**, 94–105.
37. Taori, A., Taylor, M. J. and Franke, S., Terdiurnal wave signatures in the upper mesospheric temperature and their association with the wind fields at low latitudes (20°N). *J. Geophys. Res.*, 2005, **110**, D09S06; doi:10.1029/2004JD004564.
38. Viereck, R. A. and Deehr, C. S., On the interaction between gravity waves and the OH meinel (6-2) and O_2 atmospheric (0-1) bands in the polar night airglow. *J. Geophys. Res.*, 1989, **94**, 5397–5404.

39. Drob, D. P., Ground-based optical detection of atmospheric waves in the upper mesosphere and lower thermosphere. Ph D thesis, University of Michigan, Ann Arbor, MI, 1996.
40. Reisin, E. R. and Scheer, J., Vertical propagation of gravity waves determined from zenith observations of airglow. *Adv. Space Res.*, 2001, **27**(10), 1743–1748.
41. Reisin, E. R. and Scheer, J., Gravity wave activity in the mesopause region from airglow measurements at El Leoncito. *J. Atmos. Sol.–Terr. Phys*., 2004, **66**, 655–661.
42. Taylor, M. J., Gardner, L. C. and Pendleton Jr, W. R., Long-period wave signatures in mesospheric OH meinel (6, 2) band intensity and rotational temperature at mid-latitudes. *Adv. Space Res*., 2001, **27**, 1171–1179.
43. Lopez-Gonzalez, M. J. *et al.*, Tidal variations of O_2 atmospheric and OH (6-2) airglow and temperature at mid-latitude from SATI observations. *Ann. Geophys*., 2005, **23**, 3579–3590.
44. Aushev, V. M., Lyahov, V. V., Lopez-Gonzalez, M. J., Shepherd, M. G. and Dryna, E. A., Solar eclipse of the 29 March 2006: results of the optical measurements by MORTI over Almaty (43.03°N, 76.58°E). *J. Atmos. Sol.–Terr. Phys*., 2008, **70**, 1088–1101.
45. Offermann, D., Friedrich, V., Ross, P. and Zahn, U., Neutral gas composition measurements between 80 and 120 km. *Planet. Space Sci*., 1981, **29**, 747–764.
46. Walterscheid, R. L. and Schubert, G., A dynamical–chemical model of fluctuations in the OH airglow driven by migrating tides, stationary tides and planetary waves. *J. Geophys. Res*., 1995, **100**, 17443–17449,
47. Yee, J.-H., Crowley, G., Roble, R. G., Skinner, W. R., Burrage, M. D. and Hays, P. B., Global simulations and observations of $O(^1S)$, O_2 and OH mesospheric nightglow emissions. *J. Geophys. Res*., 1997, **102**, 949–968.
48. Hickey, M. P., Schubert, G. and Walterscheid, R. L., Gravity wave driven fluctuations in the O_2 atmospheric (0-1) nightglow from an extended, dissipative emission region. *J. Geophys. Res*., 1993, **98**, 13717–13729.

ACKNOWLEDGEMENTS. This work was carried out with funds provided by the Ministry of Science and Technology, Government of India. We thank the Director, Indian Institute of Geomagnetism (IIG), Navi Mumbai for encouragement to carry out this work. The night airglow observations at Kolhapur were carried out under the scientific collaboration programme (MoU) between IIG and Shivaji University, Kolhapur. We also thank the anonymous reviewer for valuable suggestions that helped improve the manuscript.

Received 18 April 2014; revised accepted 5 January 2015

Dynamical model of daily CO concentration over Delhi: assessment of forecast potential

Jurismita Baruah and Prashant Goswami*

CSIR Fourth Paradigm Institute (Formerly C-MMACS), Belur Campus, Wind Tunnel Road, Bengaluru 560 037, India

Advance and accurate forecasts of air pollutant concentrations have many applications at different scales, from traffic planning to health advisories. However, such models need to incorporate local factors and must be validated against local observations for applicability. It has been shown earlier that a dynamical model successfully simulates, in forecast mode, the observed (CPCB, India) daily concentrations of SPM, RSPM, SO_2 and NO_2 over Delhi. The present work shows that the model skill is also significant in predicting CO. Together with our earlier results, the present work to the robustness and enhanced scope of dynamical forecast of air pollution.

Keywords: Air pollution, carbon monoxide, dynamical model, mesoscale forecast.

ACCURATE simulation of pollutant concentrations over an air basin is important for many applications like estimation of emission loads, overall health risk assessment and traffic planning[1]. Air pollution model with sufficient skill can also be used to assess how pollutant levels would change in response to changes in emission rate[2]. Worldwide there have been efforts to develop and validate such air pollution models at different scales. As the pollutant concentrations over an air basin like a mega city strongly depend on the local emission processes, an air pollution model needs to incorporate the relevant local processes in its formulation. In urban areas vehicle, industries, windblown dust and domestic appliances are recognized as major sources of air pollution. However, relative contributions of these sources vary from one location to another.

Delhi, as a growing mega city, has seen manyfold increase in its industrial, vehicular as well as domestic emissions[3]. The growing emission has serious environmental and societal implications related to ecological unbalance and environmental degradation. In recent years, transportation systems are growing at an unprecedented rate. Mobile source emissions are the maximum contributors of carbon monoxide (CO) in Delhi[4,5]. Literature analysis reveals that CO has emerged as the main pollutant in urban centres, amounting approximately to 90% contribution through the transport sector alone[6]. Thus, there is an urgent need to develop a dynamical model

*For correspondence. (e-mail: goswami@cmmacs.ernet.in)